JOURNAL OF GUIDANCE, CONTROL, AND DYNAMICS
Vol. 38, No. 4, April 2015

Adaptive Control for Aircraft Longitudinal Dynamics with Thrust Saturation

Francisco Gavilan,* Rafael Vazquez,† and José Á. Acosta‡
Universidad de Sevilla, 41092 Seville, Spain

DOI: 10.2514/1.G000028

An output-feedback control law is designed for the longitudinal flight dynamics of an aircraft. The proposed control law is designed using the adaptive backstepping method and does not require any knowledge of aircraft aerodynamics beyond well-known qualitative physical properties. The resulting feedback controller is able to follow given references in both airspeed and flight-path angle by actuating elevator deflections and aircraft engine thrust. Engine physical limits are incorporated into the design by using a Lyapunov function analysis that includes saturation, obtaining a novel hybrid adaptation law that guarantees closed-loop system stability. Simulation results show good performance of the feedback law and, in particular, demonstrate that the hybrid adaptation law improves the behavior of the closed-loop system when saturations are present. A degraded scenario (a sudden cargo displacement that renders the aircraft statically unstable) is also considered to show the adaptation capabilities of the control law. The simulations are carried out using a realistic aircraft model that is also developed in the paper.

Nomenclature

C_D, C_L, C_m	=	drag, lift, and pitch moment coefficients
C_{D_0}, k_1, k_2	=	drag model coefficients
$C_{m_{(\cdot)}}$	=	pitch moment model coefficient
$\bar{c}$	=	mean chord, m
D	=	drag, N
F_T	=	thrust, N
g	=	acceleration of gravity, m/s^2
I_y	=	y-axis inertia, kg $\cdot$ m^2
L	=	lift, N
M	=	pitch moment, N $\cdot$ m
m	=	aircraft mass, kg
q	=	pitch angular velocity, rad/s
S	=	wing surface, m^2
V	=	airspeed, m/s
W	=	Lyapunov function
x_B, y_B, z_B	=	Cartesian coordinates in body axes, m
$\boldsymbol{y}$	=	measurable output vector
z	=	error variable
α	=	angle of attack, deg
α_0	=	trim angle of attack, deg
β_V, β_γ	=	known parameters depending on physical properties of the aircraft
δ_e	=	elevator deflection, deg
$\boldsymbol{\varphi}$	=	vector of measurable parameters
γ	=	flight-path angle, deg
ρ	=	air density, kg/m^3
θ	=	pitch angle, deg
$\boldsymbol{\theta}$	=	vector of unknown parameters

I. Introduction

UNMANNED aerial vehicles (UAVs) are receiving considerable attention from both industry and academia due to the many advantages they possess over traditional aircraft. Obviously, the main advantage is the lack of an onboard pilot. Not needing a pilot makes the aircraft lighter, cheaper, and better suited for a wide range of missions in hazardous scenarios in both military and civil missions (such as surveillance or reconnaissance). Although some UAVs are remotely flown by human pilots, oftentimes autonomous flight capabilities are necessary. Thus, it is required to design onboard automatic flight control systems for UAVs with good performance and versatility. Even in the case of remotely controlled UAVs, having an automatic flight controller is desirable, at least as a backup system.

However, the design of automatic flight controllers is far from trivial. One of the main difficulties is the absence of precise mathematical models valid for relevant flight conditions. Aerodynamic forces and moments are highly nonlinear and difficult to model accurately. The traditional approach to overcome this problem is the use of linearized aircraft models around a selected flight condition. Numerous classical linear control techniques can then be applied (see, for instance, [1]). However, if the state of the aircraft is too different from the flight condition used for design, the model might fail to accurately capture the system behavior. In this situation, linear control laws can be prone to misbehavior or even failure. The gain scheduling technique (see [2]) tackles this problem by computing a set of controllers, each of them computed for a given flight condition. Then, the appropriate feedback is found by interpolating among the controllers according to the aircraft state. This technique has been widely applied in the aerospace industry (see [3] for a survey). However, the computation of gain scheduling controllers requires the estimation of aircraft stability derivatives for a sufficiently large number of flight conditions, which can be a cumbersome task.

Nonlinear control techniques have the potential for avoiding these problems. For instance, feedback linearization (see [4,5]) is a method that allows the design of feedback laws valid for all the flight envelope. However, an accurate model is still required. The backstepping technique (see [6]) lends itself naturally to the design of flight controllers given the cascade structure of flight dynamics. In the presence of parametric uncertainties, adaptive backstepping allows one to design adaptive controllers without knowledge of model parameters. For instance, Härkegård has presented an adaptive backstepping design in [7], complemented with a control allocation method to compute actuator values. Another example is in [8], which introduces an adaptive backstepping controller for an F-16 model; in that work, aerodynamics are modeled with neural networks whose weights are estimated using adaptation laws. A similar approach for quadrotor flight control is presented in [9].

Another promising design technique based on adaptive backstepping is the method of command filters (see [10]). These are user-defined filters whose inputs are the control signals obtained from

Received 10 May 2013; revision received 7 November 2013; accepted for publication 19 November 2013; published online 9 April 2014.

*Assistant Professor, Department of Aerospace Engineering, Escuela Técnica Superior de Ingeniería; fgavilan@us.es.

†Professor, Department of Aerospace Engineering, Escuela Técnica Superior de Ingeniería; rvazquez1@us.es.

‡Professor, Departamento de Ingeniería de Sistemas y Automática, Escuela Técnica Superior de Ingeniería; jaar@us.es.

backstepping and whose outputs are both filtered control signals and their derivatives. Command filters allow one to explicitly consider actuator limitations (such as saturations or maximum rates of change) and provide virtual control derivatives as output signals (which is useful because they are required for backstepping control laws). However, the method does not guarantee exact convergence of derivatives as standard adaptive backstepping (see [11] for details). Exact results are available when parameters are known (see [12]) and for certain classes of single input/single output systems without constraints (as shown in [11]). Despite this theoretical shortcoming, command filters have proven themselves quite successful in experiments (see, for instance, [13–15]).

Outside of backstepping, other adaptive and modelless schemes are also available. For instance, in [16], a parameter estimator is constructed through the use of invariant manifolds. Another technique is extremum seeking (see [17]), which introduces artificial disturbances in the system input to find a control signal that steers a given cost function to its minimum. Although extremum seeking has been mostly applied to process and reaction systems (see the survey [18]), a number of aerospace applications have been developed, such as in [19] (which considers the problem of formation flying) or [20] (which uses atmospheric turbulence as the input disturbance to optimize aircraft endurance). However, these designs do not take into account input saturation. Another adaptive approach is the method known as "control hedging," which allows one to take saturations into account in the adaptation law. In [21], this method is used, together with dynamic inversion and control allocation, to design a flight controller for a fighter aircraft.

This work presents a novel nonlinear output-adaptive feedback control design for aircraft longitudinal dynamics. The resulting feedback law is suitable for conventional airplanes operating in normal flight conditions and is able to follow commanded references in both aerodynamic velocity and flight-path angle. The controller uses elevator deflections and engine thrust level as actuators and requires only a minimal knowledge of the aircraft aerodynamics (qualitative properties). It is assumed that the airplane is equipped with inertial sensors, GPS, and an air-data system to provide the required measurements. Engine thrust saturation is explicitly considered in the design, resulting in a hybrid adaptation law with proven stabilization properties. The obtained feedback and adaptation laws are rather explicit and simple, and therefore well suited to implementation. Additionally, simulation results are provided to show the performance of the control law for a nonlinear UAV model, developed by using a combination of DATCOM (see [22]) and vortex lattice analysis (as described in [23]). The model also includes actuator saturations and rate limits. Details of the nonlinear aerodynamic model are included in the Appendix. The simulations include a degraded scenario (a sudden cargo displacement that renders the aircraft statically unstable) to show the adaptation capabilities of the control law.

The basis of this work can be found in the conference papers [24,25]. The first conference paper contains the initial attempt to solve the problem using a full-state feedback design. In that paper, the trim angle of attack (which depends on the lift coefficient) and the aerodynamic coefficient $C_{m_{\delta_e}}$ (which multiplies the elevator deflection actuation) were assumed known. The assumption was dropped in [25], leading to an output-feedback adaptive control law. The present paper contains a redesign of the velocity controller and adaptation law to handle engine thrust saturation, which posed a more challenging control problem. This redesign has led to a simpler formulation of the control law and a nontrivial hybrid adaptation law able to handle engine saturation while still guaranteeing system stability.

The paper is structured as follows. Section II begins by introducing the aircraft model. Next, Sec. III details the controller design, which is divided into two parts. First, the design of the velocity controller is considered; then, the design of the flight-path angle controller is explained. The performance of the joint controller is then shown by simulation in Sec. IV. Section V concludes the paper with some observations. A description of the simulation model is also included in the Appendix at the end of the paper.

II. Aircraft Longitudinal Flight Model

Following [26], the longitudinal equations of motion of flight mechanics are

$$\dot{V} = \frac{1}{m}(-D + F_T \cos\alpha - mg \sin\gamma) \tag{1}$$

$$\dot{\gamma} = \frac{1}{mV}(L + F_T \sin\alpha - mg \cos\gamma) \tag{2}$$

$$\dot{\theta} = q \tag{3}$$

$$\dot{q} = \frac{M(\delta_e)}{I_y} \tag{4}$$

where V is the airspeed, γ is the flight-path angle, θ is the pitch angle, q is the pitch angular velocity, F_T is the engine thrust, δ_e is the elevator angle, m and I_y are the mass and the inertia, and L, D, and $M(\delta_e)$ represent aerodynamic lift, drag, and pitch moment, respectively. Some of these variables are shown in Fig. 1.

In the longitudinal model, the angle of attack α is related to γ and θ as follows

$$\alpha = \theta - \gamma \tag{5}$$

As usual, to model lift, drag, and aerodynamic moment, the following nondimensional coefficients are defined:

$$L = \frac{1}{2}\rho V^2 S C_L, \qquad D = \frac{1}{2}\rho V^2 S C_D, \qquad M = \frac{1}{2}\rho V^2 S \bar{c} C_m(\delta_e) \tag{6}$$

with S being the reference wing surface, ρ the air density, $\bar{c}$ the mean chord, and C_L, C_D, and $C_m(\delta_e)$ the lift, drag, and pitch moment coefficients, respectively. Following classical references (such as [27]), the drag and moment coefficients can be modeled as

$$C_D = C_{D_0} + k_1 C_L + k_2 C_L^2 \tag{7}$$

$$C_m(\delta_e) = C_{m_0} + C_{m_\alpha}\alpha + C_{m_q} q + C_{m_{\delta_e}}\delta_e \tag{8}$$

where C_{D_0}, k_1, k_2, C_{m_0}, C_{m_α}, C_{m_q}, and $C_{m_{\delta_e}}$ are aerodynamic coefficients. In this work, it is assumed that $C_{m_{\delta_e}} < 0$. The sign of this coefficient is determined by the aircraft configuration. Note that these models are only used for control design purposes (Sec. III). For simulations (Sec. IV), the more realistic model shown in the Appendix is employed.

Only the following weak assumption is considered for the lift coefficient, which can be considered a good approximation for conventional airplanes operating in normal flight regimes (this paper does not address high-performance airplanes performing aggressive maneuvers).

Assumption 2.1: The aircraft lift coefficient C_L is only a function of α. In addition, choosing the reference axis x_B in Fig. 1 so that $C_L(0) = 0$ (i.e., x_B is parallel to the aircraft zero-lift line), the property $\alpha \cdot C_L(\alpha) \geq 0$ is satisfied for all meaningful values of α.

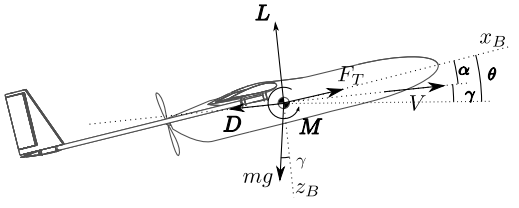

Fig. 1 Definition of forces, moments, and angles.

III. Controller Design

The control objective is the design of a feedback law to follow given references in velocity V_r and flight-path angle γ_r. For design purposes, the longitudinal motion is split into the velocity dynamics [given by Eq. (1)] and the flight-path angle dynamics (pitch dynamics, given by Eqs. (2–4)]. Two separate controllers are designed: The aerodynamic velocity is controlled using only engine thrust F_T and the flight-path angle is controlled by actuating the elevator angle δ_e. It is assumed that the aircraft has a GPS and inertial measurement unit (IMU) in conjunction with an air-data system, from which the necessary measurements of attitude angles, pitch angular velocity, airspeed, and angle of attack are obtained with enough accuracy.

A. Control of Aerodynamic Velocity

Substituting the drag model D from Eq. (6) into Eq. (1), one has

$$\dot{V} = \frac{1}{m}\left(-\frac{1}{2}\rho V^2 S C_D + F_T \cos\alpha - mg \sin\gamma\right) \tag{9}$$

with α and γ measurable and the engine thrust F_T as a control input. Including the drag model (7) and defining the error $z_V := V - V_r$, the dynamics of z_V is given by

$$\begin{aligned}\dot{z}_V &= -\frac{1}{2m}\rho(z_V + V_r)^2 S\boldsymbol{\varphi}_V(\alpha)^T \cdot \boldsymbol{\theta}_V + F_T\frac{\cos\alpha}{m} - g\sin\gamma - \dot{V}_r \\ &= -\beta_V(z_V^2 + V_r^2 + 2z_V V_r)\boldsymbol{\varphi}_V(\alpha)^T \cdot \boldsymbol{\theta}_V \\ &\quad + F_T\frac{\cos\alpha}{m} - g\sin\gamma - \dot{V}_r \end{aligned} \tag{10}$$

where $\boldsymbol{\theta}_V \in \mathbb{R}^3$ is a vector of unknown parameters and $\boldsymbol{\varphi}_V \in \mathbb{R}^3$ is a measurable vector defined as

$$\boldsymbol{\varphi}_V(\alpha) := [\,1 \quad \alpha \quad \alpha^2\,]^T, \qquad \boldsymbol{\theta}_V := [\,C_{D_0} \quad k_1 \quad k_2\,]^T \tag{11}$$

so that drag model (7) becomes $C_D = \boldsymbol{\varphi}_V(\alpha)^T \cdot \boldsymbol{\theta}_V > 0$. In system (10), the parameter

$$\beta_V := \frac{\rho S}{2m} > 0$$

has also been defined.

Next, a basic controller design that steers z_V to zero is presented. This design does not take into account engine saturation, a limitation that is addressed subsequently.

1. Velocity Controller Design Without Considering Thrust Saturation

The control law is summarized in the following proposition.

Proposition 3.1 (Velocity control law, thrust without saturation): Consider the system (10) and let $\hat{\boldsymbol{\theta}}_V$ be the estimate of $\boldsymbol{\theta}_V$ defined in Eq. (11). The adaptive-state feedback law given by

$$F_T = \frac{m}{\cos\alpha}(g\sin\gamma + \dot{V}_r + \beta_V V_r^2 \boldsymbol{\varphi}(\alpha)^T \cdot \hat{\boldsymbol{\theta}}_V - \kappa_{V_1} z_V) \tag{12}$$

$$\dot{\hat{\boldsymbol{\theta}}}_V = -\beta_V z_V V_r^2 \boldsymbol{\Gamma}_V \boldsymbol{\varphi}_V(\alpha) \tag{13}$$

where the controller gain and the adaptation gain matrix satisfy, respectively, $\kappa_{V_1} > 0$ and $\boldsymbol{\Gamma}_V = \boldsymbol{\Gamma}_V^T > 0$, guarantees global boundedness of z_V and $\hat{\boldsymbol{\theta}}_V$ and convergence of z_V to zero.

Proof: Define the following Lyapunov function:

$$W_V = \frac{1}{2}z_V^2 + \frac{1}{2}\tilde{\boldsymbol{\theta}}_V^T \boldsymbol{\Gamma}_V^{-1}\tilde{\boldsymbol{\theta}}_V \tag{14}$$

where $\tilde{\boldsymbol{\theta}}_V := \boldsymbol{\theta}_V - \hat{\boldsymbol{\theta}}_V$ is the estimation error vector. Thus, the derivative with respect to time of Eq. (14) along the trajectories of system (10) reads

$$\begin{aligned}\dot{W}_V &= z_V\left(-\beta_V(z_V + V_r)^2\boldsymbol{\varphi}_V(\alpha)^T \cdot \boldsymbol{\theta}_V + F_T\frac{\cos\alpha}{m} - g\sin\gamma - \dot{V}_r\right) \\ &\quad + \tilde{\boldsymbol{\theta}}_V^T\boldsymbol{\Gamma}_V^{-1}\dot{\tilde{\boldsymbol{\theta}}}_V \\ &= -\beta_V 2z_V^2 V_r\boldsymbol{\varphi}_V(\alpha)^T \cdot \boldsymbol{\theta}_V - z_V\beta_V z_V^2\boldsymbol{\varphi}_V(\alpha)^T \cdot \boldsymbol{\theta}_V \\ &\quad - z_V\left(\beta_V V_r^2\boldsymbol{\varphi}_V(\alpha)^T \cdot \boldsymbol{\theta}_V - F_T\frac{\cos\alpha}{m} + g\sin\gamma + \dot{V}_r\right) \\ &\quad - \tilde{\boldsymbol{\theta}}_V^T\boldsymbol{\Gamma}_V^{-1}\dot{\hat{\boldsymbol{\theta}}}_V \end{aligned} \tag{15}$$

where F_T has been replaced by control law (12).

Using the positiveness of the aerodynamic velocity, the velocity error $z_V = V - V_r$ must satisfy $z_V \geq -V_r$, which also can be written as $-z_V \leq V_r$. Furthermore, taking into account the definition of the drag coefficient (which is positive) $C_D = \boldsymbol{\varphi}_V(\alpha)^T \cdot \boldsymbol{\theta}_V \geq 0$, the second term of $\dot{W}_V$ can be bounded as

$$-z_V\beta_V z_V^2\boldsymbol{\varphi}_V(\alpha)^T \cdot \boldsymbol{\theta}_V \leq \beta_V z_V^2 V_r\boldsymbol{\varphi}_V(\alpha)^T \cdot \boldsymbol{\theta}_V \tag{16}$$

and then the time derivative of the Lyapunov function reads

$$\begin{aligned}\dot{W}_V &\leq -\beta_V z_V^2 V_r\boldsymbol{\varphi}_V(\alpha)^T \cdot \boldsymbol{\theta}_V \\ &\quad - z_V\left(\beta_V V_r^2\boldsymbol{\varphi}_V(\alpha)^T \cdot \boldsymbol{\theta}_V - F_T\frac{\cos\alpha}{m} + g\sin\gamma + \dot{V}_r\right) \\ &\quad - \tilde{\boldsymbol{\theta}}_V^T\boldsymbol{\Gamma}_V^{-1}\dot{\hat{\boldsymbol{\theta}}}_V \end{aligned} \tag{17}$$

Introducing now the control law (12) and the adaptation law (13), one has

$$\dot{W}_V \leq -\beta_V z_V^2 V_r\boldsymbol{\varphi}_V(\alpha)^T \cdot \boldsymbol{\theta}_V - \kappa_{V_1} z_V^2 \leq 0 \tag{18}$$

Thus, because W_V is positive definite and radially unbounded and $\dot{W}_V \leq 0$ then, by the LaSalle–Yoshizawa theorem, global boundedness of z_V and $\hat{\boldsymbol{\theta}}_V$ is concluded, and convergence of z_V to zero. □

The velocity controller of Proposition 3.1 improves the one previously presented by the authors in [24]. This new feedback law is able to achieve global stability using a simpler control law with a lower computational burden. In addition, this simpler formulation enables the possibility of dealing with saturations in the control signal (i.e., the thrust) with only minor modifications. This is addressed next.

2. Velocity Controller Design Considering Thrust Saturation

The assumption that the engine can provide any amount of thrust demanded by the velocity control law is here dropped. Calling $\bar{F}_T$ the maximum thrust (and assuming the minimum thrust is zero), one has then that $F_T \in [0, \bar{F}_T]$. To be able to reach the reference, the following assumption is also considered.

Assumption 3.1: The reference flight condition (given by γ_r and V_r) can be attained without violating the engine thrust limitation.

This assumption can be mathematically stated by considering the equilibrium solution in system (10). One reaches

$$0 = -\beta_V V_r^2\boldsymbol{\varphi}_V(\alpha)^T \cdot \boldsymbol{\theta}_V + F_T\frac{\cos\alpha}{m} - g\sin\gamma - \dot{V}_r \tag{19}$$

The equation should be satisfied for $F_T \in [0, \bar{F}_T]$, which implies

$$\beta_V V_r^2\boldsymbol{\varphi}_V(\alpha)^T \cdot \boldsymbol{\theta}_V + g\sin\gamma + \dot{V}_r \in \left[0, \bar{F}_T\frac{\cos\alpha}{m}\right] \tag{20}$$

Therefore, the following two inequalities hold:

$$\beta_V V_r^2\boldsymbol{\varphi}_V(\alpha)^T \cdot \boldsymbol{\theta}_V + g\sin\gamma + \dot{V}_r \geq 0 \tag{21}$$

$$\beta_V V_r^2 \boldsymbol{\varphi}_V(\alpha)^T \cdot \boldsymbol{\theta}_V + g \sin\gamma + \dot{V}_r \le \bar{F}_T \frac{\cos\alpha}{m} \tag{22}$$

Next, the closed-loop system behavior in case of saturation is analyzed in the two possible scenarios: maximum and minimum thrust limits. The same Lyapunov function (14) is used as a base to implement modifications to the control and adaptation laws.

Case 1: $F_T = \bar{F}_T$.

If the control law is demanding a thrust higher than $\bar{F}_T$, then considering the control law (12), one obtains

$$\frac{m}{\cos\alpha}(g \sin\gamma + \dot{V}_r + \beta_V V_r^2 \boldsymbol{\varphi}(\alpha)^T \cdot \hat{\boldsymbol{\theta}}_V - \kappa_{V_1} z_V) \ge \bar{F}_T \tag{23}$$

which is equivalent to

$$\beta_V V_r^2 \boldsymbol{\varphi}(\alpha)^T \cdot \hat{\boldsymbol{\theta}}_V - \bar{F}_T \frac{\cos\alpha}{m} + g \sin\gamma + \dot{V}_r \ge \kappa_{V_1} z_V \tag{24}$$

One cannot use the Lyapunov derivative bound obtained in Eq. (18), because the control law cannot be substituted in Eq. (17). Thus, $\dot{W}_V$ is now obtained as

$$\begin{aligned}\dot{W}_V \le & -\beta_V z_V^2 V_r \boldsymbol{\varphi}_V(\alpha)^T \cdot \boldsymbol{\theta}_V \\ & - z_V \times \left(\beta_V V_r^2 \boldsymbol{\varphi}_V(\alpha)^T \cdot \boldsymbol{\theta}_V - \bar{F}_T \frac{\cos\alpha}{m} + g \sin\gamma + \dot{V}_r\right) \\ & - \tilde{\boldsymbol{\theta}}_V^T \boldsymbol{\Gamma}_V^{-1} \dot{\hat{\boldsymbol{\theta}}}_V\end{aligned} \tag{25}$$

and, considering Eq. (22), the negativeness of the parentheses in the first line of Eq. (25) can be deduced. To study the system stability, it is necessary to consider two cases separately, depending on the sign of the velocity error:

Case 1.1: $z_V \ge 0$.

In this case, the original adaptation law (13) can be used. Thus, one gets

$$\begin{aligned}\dot{W}_V \le & -\beta_V z_V^2 V_r \boldsymbol{\varphi}_V(\alpha)^T \cdot \boldsymbol{\theta}_V \\ & - z_V \left(\beta_V V_r^2 \boldsymbol{\varphi}_V(\alpha)^T \cdot \hat{\boldsymbol{\theta}}_V - \bar{F}_T \frac{\cos\alpha}{m} + g \sin\gamma + \dot{V}_r\right)\end{aligned} \tag{26}$$

and considering the bound Eq. (24) together with the positiveness of z_V, one finally reaches

$$\dot{W}_V \le -\beta_V z_V^2 V_r \boldsymbol{\varphi}_V(\alpha)^T \cdot \boldsymbol{\theta}_V - \kappa_{V_1} z_V^2 \tag{27}$$

Case 1.2: $z_V < 0$.

In this case, the adaptation law is stopped (making $\dot{\hat{\boldsymbol{\theta}}} = 0$). Thus, the time derivative of the Lyapunov function becomes

$$\begin{aligned}\dot{W}_V \le & -\beta_V z_V^2 V_r \boldsymbol{\varphi}_V(\alpha)^T \cdot \boldsymbol{\theta}_V \\ & - z_V \left(\beta_V V_r^2 \boldsymbol{\varphi}_V(\alpha)^T \cdot \boldsymbol{\theta}_V - \bar{F}_T \frac{\cos\alpha}{m} + g \sin\gamma + \dot{V}_r\right) \\ \le & -\beta_V z_V^2 V_r \boldsymbol{\varphi}_V(\alpha)^T \cdot \boldsymbol{\theta}_V\end{aligned} \tag{28}$$

where Eq. (22) has been used, making the parentheses in the first line of Eq. (28) negative.

Thus, in case 1, $\dot{W}_V$ is negative semidefinite for any value of z_V.

Case 2: $F_T = 0$.

If the control law demands negative thrust values, a symmetrical situation to case 1 happens. It holds that

$$g \sin\gamma + \dot{V}_r + \beta_V V_r^2 \boldsymbol{\varphi}(\alpha)^T \cdot \hat{\boldsymbol{\theta}}_V - \kappa_{V_1} z_V \le 0 \tag{29}$$

$$\beta_V V_r^2 \boldsymbol{\varphi}_V(\alpha)^T \cdot \boldsymbol{\theta}_V + g \sin\gamma + \dot{V}_r \ge 0 \tag{30}$$

where the first inequality is due to control law (12), and the second one is implied by Eq. (21). Moreover, it can be seen that the Lyapunov function derivative is now bounded as

$$\begin{aligned}\dot{W}_V \le & -\beta_V z_V^2 V_r \boldsymbol{\varphi}_V(\alpha)^T \\ & \cdot \boldsymbol{\theta}_V - z_V(\beta_V V_r^2 \boldsymbol{\varphi}_V(\alpha)^T \cdot \boldsymbol{\theta}_V + g \sin\gamma + \dot{V}_r) - \tilde{\boldsymbol{\theta}}_V^T \boldsymbol{\Gamma}_V^{-1} \dot{\hat{\boldsymbol{\theta}}}_V\end{aligned} \tag{31}$$

As before, the analysis is split into two cases, depending on the sign of the velocity error variable.

Case 2.1: $z_V \le 0$.

In this case, the original adaptation law (13) is employed. Thus, one has

$$\begin{aligned}\dot{W}_V \le & -\beta_V z_V^2 V_r \boldsymbol{\varphi}_V(\alpha)^T \cdot \boldsymbol{\theta}_V \\ & - z_V(\beta_V V_r^2 \boldsymbol{\varphi}_V(\alpha)^T \cdot \hat{\boldsymbol{\theta}}_V + g \sin\gamma + \dot{V}_r)\end{aligned} \tag{32}$$

Using the bound Eq. (29) and keeping in mind that $-z_V$ is positive, the Lyapunov function derivative reads

$$\dot{W}_V \le -\beta_V z_V^2 V_r \boldsymbol{\varphi}_V(\alpha)^T \cdot \boldsymbol{\theta}_V - \kappa_{V_1} z_V^2 \tag{33}$$

which is negative semidefinite.

Case 2.2: $z_V > 0$.

In this case, the adaptation law is stopped. The time derivative of the Lyapunov function is now given by

$$\begin{aligned}\dot{W}_V & \le -\beta_V z_V^2 V_r \boldsymbol{\varphi}_V(\alpha)^T \cdot \boldsymbol{\theta}_V - z_V(\beta_V V_r^2 \boldsymbol{\varphi}_V(\alpha)^T \cdot \boldsymbol{\theta}_V + g \sin\gamma + \dot{V}_r) \\ & \le -\beta_V z_V^2 V_r \boldsymbol{\varphi}_V(\alpha)^T \cdot \boldsymbol{\theta}_V\end{aligned} \tag{34}$$

where both Eq. (30) and $-z_V \le 0$ have been used. Thus, in case 2, the Lyapunov function derivative is also negative semidefinite.

As a result of this analysis, it has been shown that a modification of the adaptation law is sufficient to make the Lyapunov function time-derivative negative semidefinite in all possible scenarios. This leads to a hybrid adaptation law that guarantees the stability of closed-loop velocity dynamics even in the presence of thrust saturation (always under the assumption of a reachable velocity reference). The result is summarized in the following proposition, whose proof follows immediately from the previous discussion.

Proposition 3.2 (Velocity control law, thrust with saturation): Consider the system (10) and let $\hat{\boldsymbol{\theta}}_V$ be the estimate of $\boldsymbol{\theta}_V$ defined in Eq. (11). Assume that, due to engine limits, the available control signal lies in the interval $F_T \in [0, \bar{F}_T]$. Then, the hybrid adaptive-state feedback law given by

$$F_T = \frac{m}{\cos\alpha}(g \sin\gamma + \dot{V}_r + \beta_V V_r^2 \boldsymbol{\varphi}(\alpha)^T \cdot \hat{\boldsymbol{\theta}}_V - \kappa_{V_1} z_V) \tag{35}$$

$$\dot{\hat{\boldsymbol{\theta}}}_V = \begin{cases} 0 & \text{if } F_T \le 0 \quad \text{and} \quad z_V \ge 0, \\ 0 & \text{if } F_T \ge \bar{F}_T \quad \text{and} \quad z_V \le 0, \\ -\beta_V z_V V_r^2 \boldsymbol{\Gamma}_V \boldsymbol{\varphi}_V(\alpha) & \text{otherwise} \end{cases} \tag{36}$$

where the controller gain and the adaptation gain matrix satisfy, respectively, $\kappa_{V_1} > 0$ and $\boldsymbol{\Gamma}_V = \boldsymbol{\Gamma}_V^T > 0$, guarantees global boundedness of z_V and $\hat{\boldsymbol{\theta}}_V$ and convergence of z_V to zero.

The hybrid adaptation law has a simple physical interpretation that deserves to be commented upon. Consider the following situation. If a sudden steep increment in the reference velocity occurs, the error variable $z_V = V - V_r$ might reach significant negative values. Then, the last term of the control law (13) might rise too much and steer the control signal into its maximum value (case 1.2). If the feedback control does not consider saturations, then the aircraft would not be accelerating as fast as supposed by the control logic. Then, the original adaptation law would lead to an artificially high drag estimation (which would be the only internal explanation for the lack of acceleration). If this drag overestimation is not mitigated, the

control law would contain an overcompensated drag coefficient, which will be present when the aircraft velocity finally reaches its reference value. Thus, the feedback law ends up using an aggressive, high-thrust response, a behavior that persists even when z_V finally changes sign. This can lead to an adverse situation in which saturation could still continue because the penultimate term of control law (12) might become dominant.

The proposed strategy overcomes this situation by stopping the adaptation law when an upper engine limit is reached and $z_V < 0$, and turning it on again when the aerodynamic velocity reaches its reference (that is, $z_V > 0$). In Sec. IV, a simulation study shows a noticeable improvement of the system response using this hybrid adaptive control law.

B. Control of the Flight-Path Angle

This section shows the design of an adaptive output-feedback controller for the flight-path angle. This controller assumes no specific models for lift and no knowledge of pitch moment model coefficients. The controller formulation is based on a previous result by the authors presented in [25]. This is, in turn, an improvement of a previous full-state design given in [24].

First, some assumptions about the reference are stated.

Assumption 3.2: As proposed in [7], it is assumed that $\cos\gamma \approx \cos\gamma_r$. Also, $\dot{\gamma}_r$ is assumed to be zero.

Using the assumption, Eq. (2) reads

$$\dot{\gamma} = f(\alpha) = f(\theta - \gamma) \tag{37}$$

where the scalar function f is defined as

$$f(\alpha) := \frac{1}{mV}\left(\frac{1}{2}\rho V^2 S C_L(\alpha) + F_T \sin\alpha - mg\cos\gamma_r\right)$$

Note the implicit dependence of $f(\alpha)$ on γ_r. Define α_0 as the trim angle of attack, which is the value of α that (for a given γ_r) makes $f(\alpha)$ zero, [i.e., $f(\alpha_0) = 0$]. In what follows, α_0 is assumed to be constant. Because the function $f(\alpha)$ is unknown, α_0 is not computable. This also implies that the pitch reference $\theta_r := \alpha_0 + \gamma_r$ is also unknown. The only known fact about f and α_0 is that, using Assumption 2.1, $f(\alpha)$ satisfies $(\alpha - \alpha_0)f(\alpha) > 0$.

Define a vector of error coordinates $z \in \mathbb{R}^3$ as

$$z = \begin{bmatrix} z_1 \\ z_2 \\ z_3 \end{bmatrix} := \begin{bmatrix} \gamma - \gamma_r \\ \theta - \gamma_r - \alpha_0 \\ q \end{bmatrix} \tag{38}$$

Note that, because α_0 is unknown, it follows that z_2 is not a measurable quantity by itself. To clarify which states and combination of states are measurable, define a measurable output vector $\boldsymbol{y} \in \mathbb{R}^3$ as

$$\boldsymbol{y} := \begin{bmatrix} \gamma - \gamma_r \\ \alpha \\ q \end{bmatrix} \equiv \begin{bmatrix} z_1 \\ z_2 - z_1 + \alpha_0 \\ z_3 \end{bmatrix} \tag{39}$$

Rewriting the pitch dynamics (2–4) in the new set of coordinates, and considering Eq. (37), the error dynamics reads

$$\dot{z}_1 = \eta(z_2 - z_1) \tag{40}$$

$$\dot{z}_2 = z_3 \tag{41}$$

$$\dot{z}_3 = \beta_\gamma[C_{m_0} + C_{m_\alpha}(z_2 - z_1 + \alpha_0) + C_{m_q} z_3 + C_{m_{\delta_e}}\delta_e] \tag{42}$$

where

$$\beta_\gamma := \frac{\rho V^2 S\bar{c}}{2I_y}$$

and

$$\eta(x) := f(x + \alpha_0) \tag{43}$$

Notice that the properties of f imply that $x \cdot \eta(x) \geq 0$. This is the only known fact about η.

The objective of the design is to find an output-feedback law that makes the origin of the error system (40–42) globally asymptotically stable. The only input is δ_e, and the measurements are $\boldsymbol{y}$. There is no knowledge of the values of η, C_{m_0}, C_{m_α}, C_{m_q}, or $C_{m_{\delta_e}}$, apart from the facts that $x \cdot \eta(x) \geq 0$ and that $C_{m_{\delta_e}}$ is negative.

The full-state problem was previously considered in [7] for the cascade structure (40–42), but using the aerodynamic moment model M as actuation. Then, a control allocation scheme was used to estimate the corresponding elevator deflections δ_e. In this work, $M(\delta_e)$ is explicitly written and obtained as a function of the physical control input δ_e, as given by Eq. (8).

Because Eqs. (40–42) is a cascade system in strict feedback form, a step-by-step backstepping design can be used.

Step 1: First, Eq. (40) is stabilized using z_2 as a "virtual" control. Defining a Lyapunov function as

$$W_{\gamma 1} = \frac{1}{2}z_1^2$$

its derivative reads $\dot{W}_{\gamma 1} = z_1\eta(z_2 - z_1)$. Select the virtual control $z_2 = u_1(z_1) = -\kappa_{\gamma_1} z_1$, where $z_1 = y_1$ is measurable. Thus,

$$\dot{W}_{\gamma 1}|_{z_2 = u_1(z_1)} = z_1\eta(-(1 + \kappa_{\gamma_1})z_1)$$

and hence $\dot{W}_{\gamma 1}|_{z_2 = u_1(z_1)}$ is negative definite for $\kappa_{\gamma_1} > -1$.

Step 2: Define now a modified error variable as a deviation of the virtual control:

$$\tilde{z}_2 := z_2 - u_1(z_1)$$

Then, Eqs. (40) and (41) become

$$\dot{z}_1 = \eta(\tilde{z}_2 - (1 + \kappa_{\gamma_1})z_1) \tag{44}$$

$$\dot{\tilde{z}}_2 = z_3 + \kappa_{\gamma_1}\eta(\tilde{z}_2 - (1 + \kappa_{\gamma_1})z_1) \tag{45}$$

Define a Lyapunov function for Eqs. (44) and (45) as

$$W_{\gamma 2} = c_1 W_{\gamma 1} + \int_0^{\tilde{z}_2 - (1+\kappa_{\gamma_1})z_1} \eta(s)\,\mathrm{d}s$$

which is positive definite by the properties of η. Then, $\dot{W}_{\gamma 2}$ is found as

$$\dot{W}_{\gamma 2} = c_1 z_1\eta + (-\eta + z_3)\eta - \eta^2 + (c_1 z_1 + z_3)\eta \tag{46}$$

where the argument of $\eta = \eta(\tilde{z}_2 - (1 + \kappa_{\gamma_1})z_1)$ has been omitted for clarity. Selecting the virtual control as $z_3 = u_2(z_1) = -c_1 z_1$, Eq. (46) becomes $\dot{W}_{\gamma 2} = -\eta^2$ and thus negative semidefinite. By LaSalle's theorem, z_1 and $\tilde{z}_2$ tend to the largest invariant set in the set $\{(z_1, \tilde{z}_2) \in \mathbb{R}^2 : \eta = 0\}$. This implies, using the property of η and Eq. (43), that $\tilde{z}_2 - (1 + \kappa_{\gamma_1})z_1 = 0$. Then, the residual dynamics is

$$\dot{z}_1 = 0 \tag{47}$$

$$\dot{\tilde{z}}_2 = -c_1 z_1 \tag{48}$$

and therefore z_1 is constant. The derivative of the states on the set is $\dot{\tilde{z}}_2 - (1 + \kappa_{\gamma_1})\dot{z}_1 = 0$, which implies $\dot{\tilde{z}}_2 = 0$. This,

together with Eq. (48), entails that the largest invariant set is $z_1 = \tilde{z}_2 = 0$. Given that W_2 is radially unbounded, the origin is globally stable and it also follows that $\gamma \to \gamma_r$, $\theta \to \theta_r$ even though θ_r is unknown (also $\alpha \to \alpha_0$ with α_0 unknown).

Note that the virtual control law does not need the function $f(\alpha)$. To avoid the need of canceling η terms in the control law, the Lyapunov function W_2 has included an integral (first introduced in [28]).

In a preliminary design [24], an additional term $\tilde{z}_2^2$ was added to $W_{\gamma 2}$. This yielded a negative term in $\tilde{z}_2^2$ in $\dot{W}_{\gamma 2}$, allowing one to conclude exponential convergence. However, this required exact knowledge of α_0 (because $\tilde{z}_2$ contains it in its definition). It is remarkable that, to obtain an output-feedback law (not needing the value of $\tilde{z}_2$), all that was necessary was omitting the $\tilde{z}_2^2$ term. However, this improvement comes at the cost of sacrificing exponential stability, which implies some loss of robustness with respect to unmodeled dynamics.

Step 3: Defining the new error coordinate $\tilde{z}_3 := z_3 - u_2(z_1)$, the system becomes

$$\dot{z}_1 = \eta \tag{49}$$

$$\dot{\tilde{z}}_2 = \tilde{z}_3 - c_1 z_1 + \kappa_{\gamma_1} \eta \tag{50}$$

$$\dot{\tilde{z}}_3 = \beta_\gamma C_{m_{\delta_e}} (\boldsymbol{\varphi}_\gamma^T \cdot \boldsymbol{\theta}_\gamma + \delta_e) - \beta_\gamma \kappa_{\gamma_3} \tilde{z}_3 + c_1 \eta \tag{51}$$

In Eq. (51), the model (8) has been used, by defining $\boldsymbol{\theta}_\gamma \in \mathbb{R}^4$ (a vector of unknown parameters) and $\boldsymbol{\varphi}_\gamma(\boldsymbol{y}) \in \mathbb{R}^4$ (a vector of measurable quantities) as

$$\boldsymbol{\theta}_\gamma := \left[\frac{C_{m_0}}{C_{m_{\delta_e}}} \frac{C_{m_\alpha}}{C_{m_{\delta_e}}} \frac{C_{m_q}}{C_{m_{\delta_e}}} \frac{1}{C_{m_{\delta_e}}} \right]^T,$$

$$\boldsymbol{\varphi}_\gamma(\boldsymbol{y}) := \begin{bmatrix} 1 \\ \alpha \\ z_3 \\ \kappa_{\gamma_3} \tilde{z}_3 \end{bmatrix} = \begin{bmatrix} 1 \\ y_2 \\ y_3 \\ \kappa_{\gamma_3}(y_3 + c_1 y_1) \end{bmatrix} \tag{52}$$

Recall that δ_e is the elevator deflection, which is the real control input of the aircraft.

Define the Lyapunov function for this step as

$$W_{\gamma 3} = W_{\gamma 2} + \frac{c_3}{2} \tilde{z}_3^2 + \frac{|C_{m_{\delta_e}}|}{2} \tilde{\boldsymbol{\theta}}_\gamma^T \boldsymbol{\Gamma}_\gamma^{-1} \tilde{\boldsymbol{\theta}}_\gamma \tag{53}$$

where $c_3 > 0$, $\boldsymbol{\Gamma}_\gamma = \boldsymbol{\Gamma}_\gamma^T > 0$ is the adaptation gain matrix, $\hat{\boldsymbol{\theta}}_\gamma$ is the estimate of $\boldsymbol{\theta}_\gamma$, and $\tilde{\boldsymbol{\theta}}_\gamma := \boldsymbol{\theta}_\gamma - \hat{\boldsymbol{\theta}}_\gamma$ is the estimation error vector.

Then the Lyapunov function derivative is

$$\dot{W}_{\gamma 3} = -\eta^2 + \tilde{z}_3 \eta + c_3 \tilde{z}_3 \beta_\gamma C_{m_{\delta_e}} (\boldsymbol{\varphi}_\gamma^T \cdot \boldsymbol{\theta}_\gamma + \delta_e) + c_3 \tilde{z}_3 c_1 \eta - c_3 \beta_\gamma \kappa_{\gamma_3} \tilde{z}_3^2 + |C_{m_{\delta_e}}| \tilde{\boldsymbol{\theta}}_\gamma^T \boldsymbol{\Gamma}_\gamma^{-1} \dot{\tilde{\boldsymbol{\theta}}}_\gamma \tag{54}$$

Defining the control and the adaptation laws as

$$\delta_e := -\boldsymbol{\varphi}_\gamma^T \cdot \hat{\boldsymbol{\theta}}_\gamma \tag{55}$$

$$\dot{\hat{\boldsymbol{\theta}}}_\gamma = -\dot{\tilde{\boldsymbol{\theta}}}_\gamma := -c_3 \beta_\gamma \tilde{z}_3 \boldsymbol{\Gamma}_\gamma \boldsymbol{\varphi}_\gamma \tag{56}$$

and selecting $c_3 = 1/c_1$, Eq. (54) yields

$$\dot{W}_{\gamma 3} = -\eta^2 + 2\tilde{z}_3 \eta - \frac{\beta_\gamma \kappa_{\gamma_3}}{c_1} \tilde{z}_3^2 \le -\left(1 - \frac{2}{\lambda}\right) \eta^2 - \left(\frac{\beta_\gamma \kappa_{\gamma_3}}{c_1} - 2\lambda \right) \tilde{z}_3^2$$

where Young's inequality has been used with the parameter λ still free. Pick $\lambda = 4$ and $\kappa_{\gamma_3} > 8c_1/\beta_\gamma$, then one gets

$$\dot{W}_{\gamma 3} \le -\frac{1}{2} \eta^2 - \frac{1}{2} \tilde{z}_3^2$$

which is a negative semidefinite function. Invoking LaSalle's theorem as in step 2, it is straightforward to see that the largest invariant set inside the set $\{(z_1, \tilde{z}_2, \tilde{z}_3) \in \mathbb{R}^3 : \eta = 0, \tilde{z}_3 = 0\}$ is the origin $z_1 = \tilde{z}_2 = \tilde{z}_3 = 0$. Also, $z_1 = \tilde{z}_2 = 0$ implies $z_2 = 0$ by the same arguments as before, and additionally $z_1 = 0$ and $\tilde{z}_3 = 0$ imply directly $z_3 = 0$. The result obtained in this section is formally summarized in the following proposition (in the original coordinates). Its proof is immediate from the three steps followed for the backstepping design.

Proposition 3.3: Consider the flight-path-angle dynamics (2–4) under Assumptions 2.1 and 3.2, with the only measurable outputs given by Eq. (39) and being $\hat{\boldsymbol{\theta}}_\gamma$ the estimate of $\boldsymbol{\theta}_\gamma$ defined in Eq. (52). Then, the adaptive output-feedback given by

$$\delta_e = -\boldsymbol{\varphi}_\gamma(\boldsymbol{y})^T \cdot \hat{\boldsymbol{\theta}}_\gamma \tag{57}$$

$$\dot{\hat{\boldsymbol{\theta}}}_\gamma = -\frac{\beta_\gamma}{c_1} (q + c_1(\gamma - \gamma_r)) \boldsymbol{\Gamma}_\gamma \boldsymbol{\varphi}_\gamma(y) \tag{58}$$

with $c_1 > 0$ and $\kappa_{\gamma_3} > 8c_1/\beta_\gamma$, $\boldsymbol{\Gamma}_\gamma = \boldsymbol{\Gamma}_\gamma^T > 0$ and

$$\boldsymbol{\varphi}_\gamma(\boldsymbol{y}) = \begin{bmatrix} 1 \\ \alpha \\ q \\ \kappa_{\gamma_3}(q + c_1(\gamma - \gamma_r)) \end{bmatrix} \tag{59}$$

guarantees global stability of (γ, θ, q) and $\hat{\boldsymbol{\theta}}_\gamma$, and convergence of (γ, θ, q) to $(\gamma_r, \theta_r, 0)$.

IV. Simulation Results

For simulation purposes, a nonlinear model of an aircraft, Cefiro UAV, has been used. Cefiro is a light aircraft designed and built at the University of Seville (Spain). The model contains nonlinear aerodynamics and actuator limitations in both value and rate of change (see the Appendix for more details). Note that, even though the velocity and flight-path angle controllers are designed separately, simulations show both controllers operating simultaneously.

The following tuning parameters have been chosen for the velocity feedback and adaptation law (35) and (36):

$$\kappa_{V_1} = 1.5, \qquad \boldsymbol{\Gamma}_V = 0.001 \mathbf{Id}_3 \tag{60}$$

The following tuning parameters have been chosen for the flight-path angle feedback and adaptation law (57) and (58):

$$\kappa_{\gamma_3} = 4; \qquad c_1 = 1.1; \qquad \boldsymbol{\Gamma}_\gamma = 0.4 \begin{bmatrix} 1 & 0 & 0 & 0 \\ 0 & 1 & 0 & 0 \\ 0 & 0 & 1 & 0 \\ 0 & 0 & 0 & 0.1 \end{bmatrix} \tag{61}$$

The following values have been selected as initial estimates of the unknown parameters:

$$\hat{\boldsymbol{\theta}}_V = [0.05 \quad 0.05 \quad 0.05]^T, \quad \hat{\boldsymbol{\theta}}_\gamma = [0.08 \quad 0.1 \quad 4 \quad -3]^T$$

These values have been chosen with a similar order of magnitude as those typically found in conventional aircraft (obtained from classical references such as [29]). However, it is important to recall that they are not directly related to the actual values of the true parameters of the aircraft, which are assumed unknown.

Figure 2 shows both velocity and flight-path angle responses, given a reference composed of several segments with constant

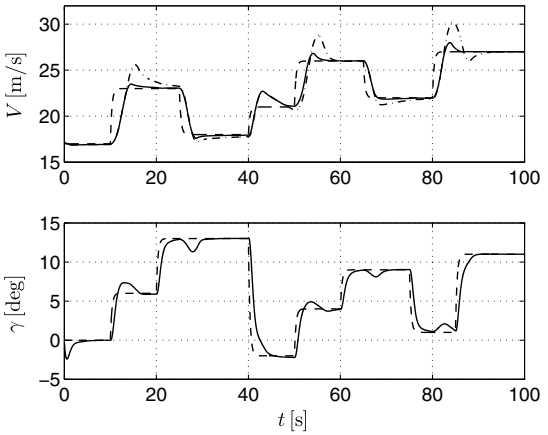

Fig. 2 Time evolution of V (solid: hybrid adaptation law including saturations; dotted: adaptation law not including saturations) and γ. Dashed lines are references.

velocity and path angle. The reference is slightly smoothed (as shown in the figure) to avoid discontinuities that would demand instantaneous changes in the control signals. Despite lack of knowledge of the aerodynamic model, both states reach their reference values with low overshoot and no steady-state error. The coupling between velocity and path angle dynamics does not seem to have any effect on the separately designed controllers. In Fig. 3, the angle of attack, the pitch angle, and the pitch angular velocity are plotted. The figure shows the control law steering the angle of attack and the pitch angle to constant (but unknown) trim values for each flight condition, at the same time that the pitch angular velocity is regulated to zero to ensure a steady straight flight.

Figure 2 also shows a noticeable improvement in the aerodynamic velocity response when taking into account thrust saturation (solid line), as compared with the simpler controller which ignores engine limitations (dash-dot line). As seen in the figure, a steep change in the reference velocity tends to steer the engine toward its limits. Saturation induces drag estimation mismatches in the adaptation law of the nonhybrid controller, which in the end produce an oscillatory behavior. On the contrary, the hybrid adaptation law is able to avoid altogether these problems by stopping the adaptation law when necessary. It is also remarkable that, although elevator saturations or limits in the rates of change of both actuators have not been taken into account in the design, their inclusion in simulations does not seem to visibly deteriorate the performance of the feedback law.

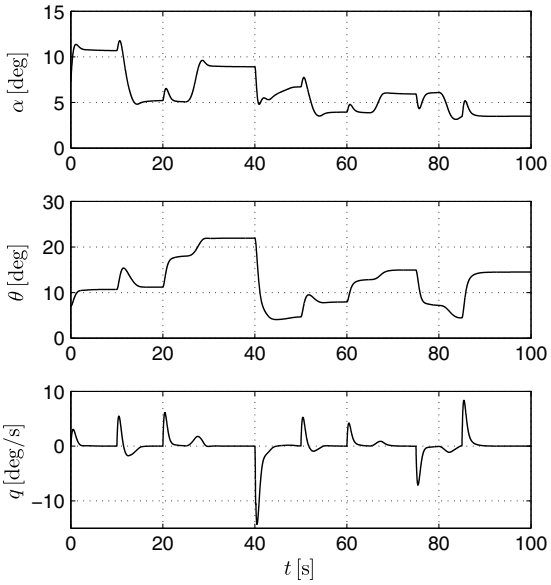

Fig. 3 Time evolution of angle of attack, pitch angle, and pitch angular velocity.

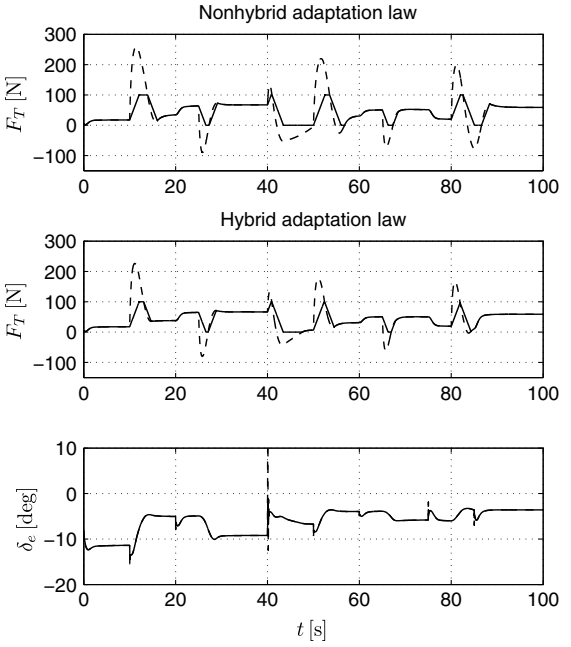

Fig. 4 Time evolution of the control signals, showing controllers with and without saturations (solid: applied; dashed: commanded).

Figure 4 depicts the computed and applied (considering the limitations in magnitude and rate of change shown in the Appendix) elevator and thrust inputs. Elevator actuation is rather smooth when moderate changes in flight-path angle are demanded, but sudden saturations may occur at steep reference changes (for instance at $t = 40$ s), in spite of which stability is not compromised. The situation with respect to the thrust is radically different due to the slower bandwidth of the engine response. When an abrupt change in the reference velocity is demanded, the system rapidly enters in saturation during a noticeable amount of time. This justifies the inclusion of thrust saturation in the adaptation law, which mitigates considerably the oscillations of the velocity, while at the same time results in a less aggressive thrust response. Note, however, that the (computed) hybrid feedback law does not always match the applied actuation, due to rate limitations. However, this does not result in undesirable behavior.

Figures 5 and 6 show the time evolution of the parameters estimated by the adaptation laws. The parameters converge to certain constant values when the references are hold constant (which are, however, distinct from the real values). During the simulation, large

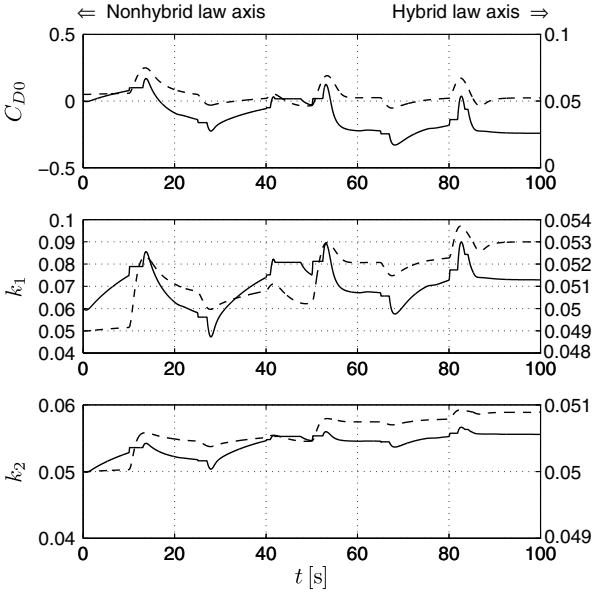

Fig. 5 Time evolution of the parameters estimated by the velocity controller (dashed: nonhybrid law, solid: hybrid law).

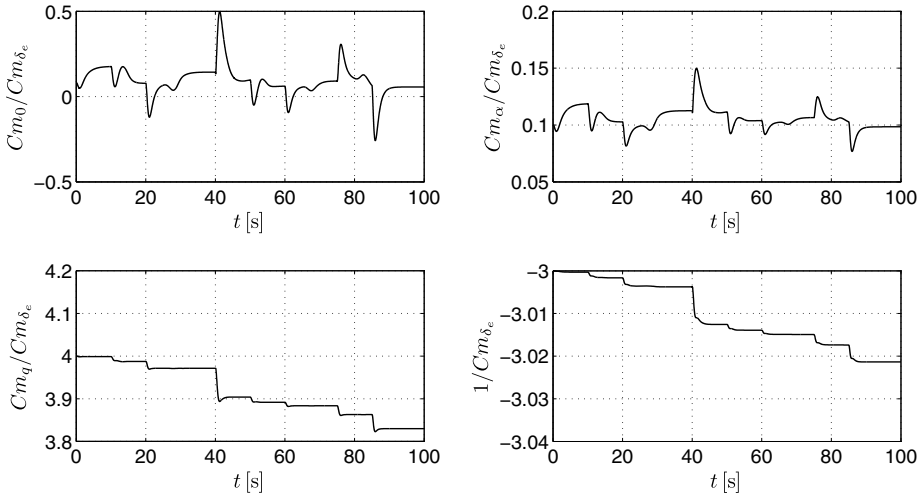

Fig. 6 Time evolution of the parameters estimated by the flight-path angle control law.

changes in the value of the estimated parameters were not observed. Figure 5 also shows the effect of including engine saturation in the adaptation laws (note the different y axis for the hybrid and nonhybrid adaptation law). When it is not included, one obtains noticeable variations in the estimated parameters which lead to drag estimation mismatches, producing oscillations in velocity as shown in Fig. 2.

To show the adaptive capability of the developed controllers, a degraded scenario is considered in which a sudden change of the airplane model occurs during the flight, modifying noticeably its handling qualities. The situation under consideration is a cargo displacement during a climb flight segment, in such a way that the center of gravity moves aft of the neutral point. This leads to a statically unstable airplane with a static margin $\mathrm{SM} = -7\%$ (implying that the derivative C_{m_α} becomes positive). The new aerodynamic coefficients for this scenario are given in the Appendix.

Figure 7 depicts the time evolution of the controlled variables V and γ. At instant $t = 30$ s, when the airplane is commanded to climb at angle $\gamma = 13$ deg, the center of gravity moves aft. This situation leads to a severe pitch-up tendency, which is immediately corrected by the control law, steering again the flight-path angle to its commanded value and regulating it properly during the remaining flight segments, even with this statically unstable behavior. As shown in Fig. 8 (where controls are plotted) the controller reacts to the cargo shift, commanding rather large elevator oscillations, while the parameters in $\boldsymbol{\theta}_\gamma$ are being adapted to the new flight condition. Once the airplane has been stabilized, the controller is able to make it follow the references in velocity and flight-path angle.

To gain more insight, in Fig. 9, one can find a zoom of the four most representative variables during the cargo shift (i.e., flight-path angle, elevator, angle of attack, and the unknown parameter $C_{m_\alpha}/C_{m_{\delta_e}}$). It can be seen that the flight-path angle controller would react to such an

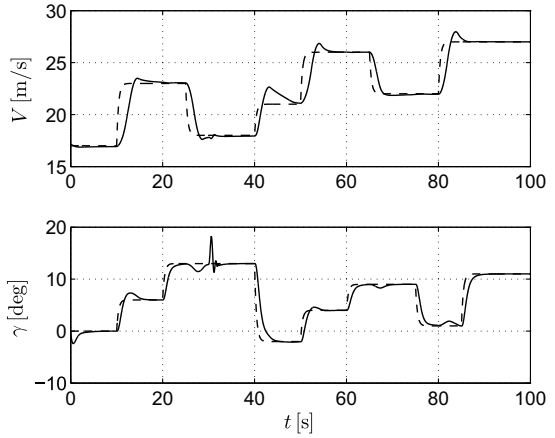

Fig. 7 Time evolution of V and γ. The cargo shift occurs at instant $t = 30$ s. Dashed lines are references.

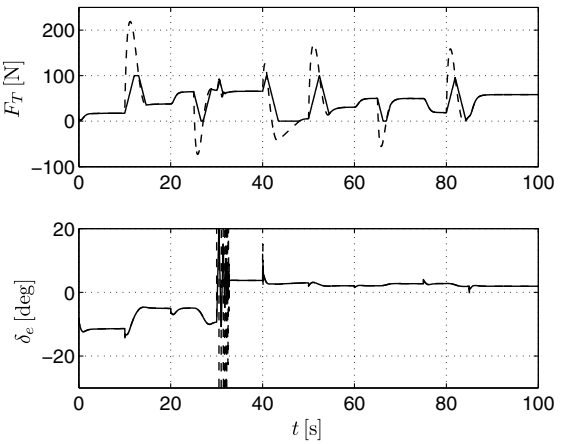

Fig. 8 Time evolution of the control signals, showing controllers with and without saturations (solid: applied; dashed: commanded). The cargo shift occurs at instant $t = 30$ s.

instantaneous change in the airplane model with an abrupt and highly oscillatory response. However, the presence of saturations in magnitude and rate of change does not allow such a behavior, and only some rather small oscillations appear in the δ_e signal. The controller is still able to stabilize the pitch-up tendency, even with the presence of these limitations. Additionally, the angle of attack is rapidly corrected, which avoids entering in stall. The change of sign in the estimated parameter $C_{m_\alpha}/C_{m_{\delta_e}}$ is also remarkable. The initial value corresponds to a statically stable airplane (so that both C_{m_α} and $C_{m_{\delta_e}}$ are negative) and afterward represents an unstable airplane with C_{m_α} positive and $C_{m_{\delta_e}}$ negative.

V. Conclusions

A novel output-adaptive feedback control law for the longitudinal flight dynamics of a UAV is proposed. The controller is able to make the aircraft follow references in velocity and flight-path angle, with minimal knowledge of aircraft aerodynamics. The design explicitly takes into account engine thrust limits. The use of Lyapunov function analysis allows one to find a stabilizing hybrid adaptive feedback law that guarantees system stability even in the presence of engine saturation. This hybrid law is compared in simulation with a previous design, which did not take into account saturations. As expected, the hybrid law performs better (when the engine is taken to its limits). A degraded scenario (a sudden cargo displacement that renders the aircraft statically unstable) is also considered to test the limits of the control law, which copes with the model change by using its adaptation capabilities.

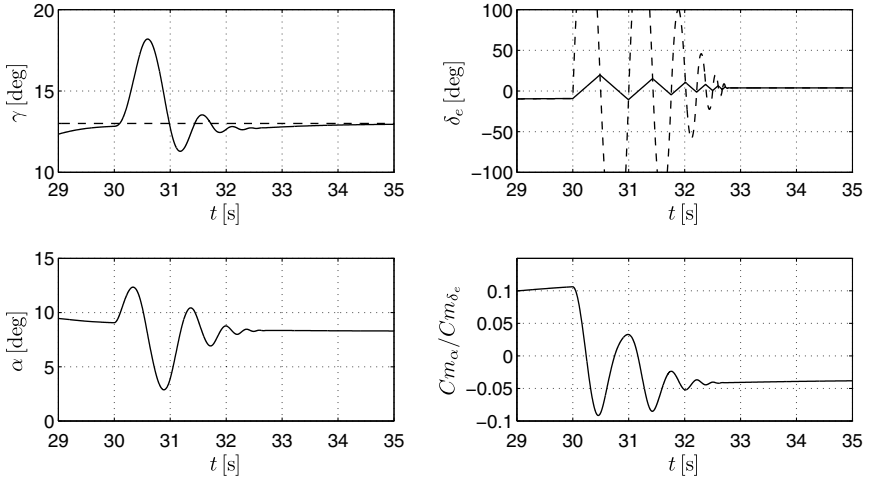

Fig. 9 Zoom of the time evolution of the flight-path angle, elevator, angle of attack, and parameter $C_{m_\alpha}/C_{m_{\delta_e}}$ when the cargo shift occurs.

The obtained control laws are simple in structure yet potent and versatile, because they have been developed on the basis of a generic aerodynamic model, which is representative of a wide variety of conventional airplanes in normal flight conditions, not even needing the computation of trim values. The explicit nature of the feedback and adaptation laws is well suited for onboard implementation. It must be noted that the controller requires measurements obtained from a GPS and IMU in conjunction with an air-data system.

It is also remarkable, looking at the seminal results on which this work is based, how a careful, yet uncomplicated, refinement of the initially selected Lyapunov functions has allowed the authors to overcome seemingly difficult challenges such as unmeasurable variables or actuator saturation.

Current research is underway to deal with elevator saturations or limits in the rates of change of both actuators. Also, whereas the proposed control law shows promising results in simulations, experimental validation would be necessary to confirm its performance.

Appendix: Simulation Model

The simulation test bed is a nonlinear model of the longitudinal dynamics of the Cefiro UAV. Cefiro is a small aircraft developed and built at the University of Seville. Some of its main characteristics are summarized in Table A1.

Table A1 Characteristics of the Cefiro aircraft

Operational weight	$m = 23$ kg
Reference cruise speed	$u_s = 19$ m/s
Wing surface	$S = 0.99$ m^2
Mean chord	$\bar{c} = 0.33$ m
Inertia moment	$I_y = 4.51$ kg $\cdot$ m^2
Engine	2.5 kW electric engine
Propeller	22×10 fixed-pitch propeller

The airplane is equipped with an IMU together with a GPS unit to obtain measurements of position, attitude angles, and linear and angular velocities. Additionally, it has an air-data boom mounted in the nose to provide accurate measurements of airspeed, static pressure, angles of attack, and sideslip.

The aircraft longitudinal model is based on the Eqs. (1–4) and requires the computation of aerodynamic forces and moments defined in Eq. (6). The coefficients are obtained using DATCOM (see [22]) complemented with a vortex lattice analysis (see [23]) for the specific geometry of the Cefiro UAV. Following DATCOM notation, lift, drag, and pitch moment coefficients are

$$C_D = C_{D_\alpha}(\alpha) + C_{D_{\delta_e}}(\alpha, \delta_e) \tag{A1}$$

$$C_L = C_{L_\alpha}(\alpha) + C_{L_{\dot\alpha}}(\alpha)\frac{\dot\alpha\,\bar{c}}{2u_s} + C_{L_q}\frac{q\bar{c}}{2u_s} + C_{L_{\delta_e}}(\delta_e) \tag{A2}$$

$$C_m = C_{m_\alpha}(\alpha) + C_{m_{\dot\alpha}}(\alpha)\frac{\dot\alpha\,\bar{c}}{2u_s} + C_{m_q}\frac{q\bar{c}}{2u_s} + C_{m_{\delta_e}}(\delta_e) \tag{A3}$$

where the functions appearing in Eqs. (A1–A3) are depicted in Figs. A1–A3, respectively. The pitch velocity effects in models (A2) and (A3) are given by the constant coefficients $C_{L_q} = 4.9240$ and $C_{m_q} = -9.0190$, respectively.

Section IV included a case in which the center of gravity moved aft of the neutral point, leading to a statically unstable airplane. To model such scenario, the aerodynamic moment coefficients have been recomputed with the new position of the center of gravity, leading to

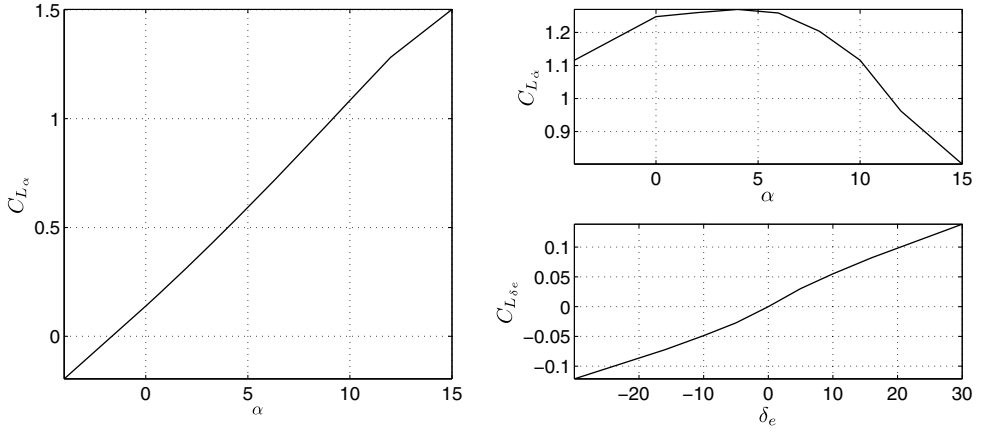

Fig. A1 Lift coefficient model of the Cefiro UAV.

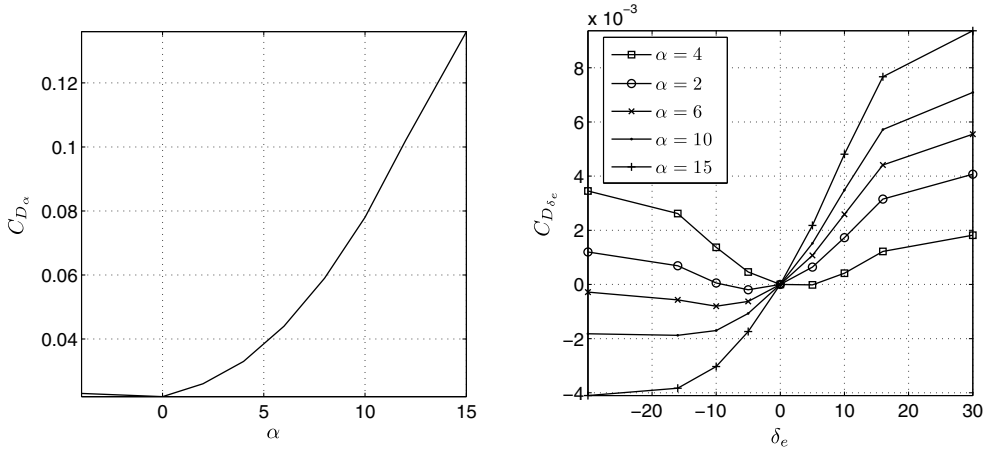

Fig. A2 Drag coefficient model of the Cefiro UAV.

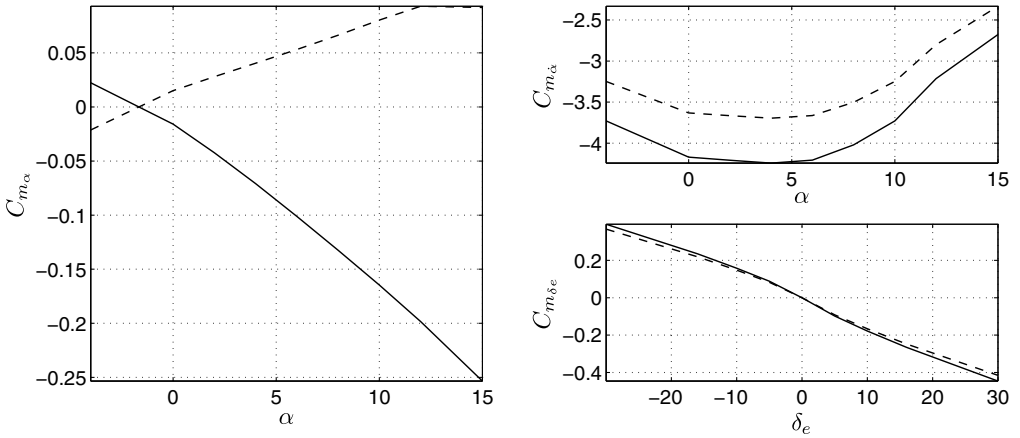

Fig. A3 Pitch moment coefficient model of the Cefiro UAV [solid line: nominal airplane (statically stable); dashed line: statically unstable airplane, after the cargo shift].

the dashed lines shown in Fig. A3 (notice the change in the slope of C_{m_α}). Additionally, the pitch angular velocity contribution to the lift and the aerodynamic moment are now given by the constants $C_{L_q} = 2.8000$ and $C_{m_q} = -7.8550$, respectively. The influence on the rest of the parameters has been considered negligible.

The following limitations in magnitude and rate of change of actuators (engine thrust and elevator angle) have also been considered in the simulation model

$$F_T \in [0, 100] \text{ N}, \qquad |\dot{F}_T| \leq 40 \text{ N/s}, \qquad |\delta_e| \leq 30 \text{ deg}, \qquad |\dot{\delta}_e| \leq 60 \text{ deg/s} \tag{A4}$$

References

[1] McLean, D., *Automatic Flight Control Systems*, Prentice–Hall, Upper Saddle River, NJ, 1990, pp. 316–418.

[2] Nichols, R. A., Reichert, R. T., and Rugh, W. J., "Gain Scheduling for H_∞ Controllers: A Flight Control Example," *IEEE Transactions on Control Systems Technology*, Vol. 1, No. 2, 1993, pp. 69–78. doi:10.1109/87.238400

[3] Rugh, W., and Shamma, J., "Research on Gain Scheduling," *Automatica*, Vol. 36, No. 10, 2000, pp. 1401–1425. doi:10.1016/S0005-1098(00)00058-3

[4] Ochi, Y., and Kanai, K., "Design of Restructurable Flight Control Systems Using Feedback Linearization," *Journal of Guidance, Control, and Dynamics*, Vol. 14, No. 5, 1991, pp. 903–911. doi:10.2514/3.20730

[5] Adams, R. J., Buffington, J. M., and Banda, S. S., "Design of Nonlinear Control Laws for High-Angle-Of-Attack Flight," *Journal of Guidance, Control, and Dynamics*, Vol. 17, No. 4, 1994, pp. 737–746. doi:10.2514/3.21262

[6] Krstić, M., Kanellakopoulos, I., and Kokotović, P., *Nonlinear and Adaptive Control Design*, Wiley, New York, 1995, pp. 29–57.

[7] Härkegård, O., "Backstepping and Control Allocation with Applications to Flight Control," Ph.D. Thesis, Linköping Univ., Linköping, Sweden, 2003.

[8] Lee, T., and Kim, Y., "Nonlinear Adaptive Flight Control Using Backstepping and Neural Networks Controller," *Journal of Guidance, Control, and Dynamics*, Vol. 24, No. 4, 2001, pp. 675–682. doi:10.2514/2.4794

[9] Das, A., Lewis, F., and Subbarao, K., "Backstepping Approach for Controlling a Quadrotor Using Lagrange Form Dynamics," *Journal of Intelligent and Robotic Systems: Theory and Applications*, Vol. 56, Nos. 1–2, 2009, pp. 127–151. doi:10.1007/s10846-009-9331-0

[10] Farrell, J., Polycarpou, M., and Sharma, M., "Adaptive Backstepping with Magnitude, Rate, and Bandwidth Constraints: Aircraft Longitude Control," *Proceedings of the American Control Conference*, Vol. 5, 2003, pp. 3898–3904.

[11] Dong, W., Farrell, J., Polycarpou, M., Djapic, V., and Sharma, M., "Command Filtered Adaptive Backstepping," *IEEE Transactions on Control Systems Technology*, Vol. 20, No. 3, 2012, pp. 566–580.

[12] Farrell, J., Polycarpou, M., Sharma, M., and Dong, W., "Command Filtered Backstepping," *IEEE Transactions on Automatic Control*, Vol. 54, No. 6, 2009, pp. 1391–1395. doi:10.1109/TAC.2009.2015562

[13] Farrell, J., Sharma, M., and Polycarpou, M., "Backstepping-Based Flight Control with Adaptive Function Approximation," *Journal of Guidance, Control, and Dynamics*, Vol. 28, No. 6, 2005, pp. 1089–1102. doi:10.2514/1.13030

[14] Sonneveldt, L., Chu, Q., and Mulder, J., "Nonlinear Flight Control Design Using Constrained Adaptive Backstepping," *Journal of Guidance, Control, and Dynamics*, Vol. 30, No. 2, 2007, pp. 322–336. doi:10.2514/1.25834

[15] Cao, L., Zhang, S., Li, X., Liu, Y., and Liu, Y., "Nonlinear Adaptive Block Backstepping Control Using Command Filter and Neural Networks Approximation," *Information Technology Journal*, Vol. 10, No. 12, 2011, pp. 2284–2291.

[16] Karagiannis, D., and Astolfi, A., "Non-Linear and Adaptive Flight Control of Autonomous Aircraft Using Invariant Manifolds," *Journal of Aerospace Engineering*, Vol. 224, No. 4, 2010, pp. 403–415.

[17] Krstic, M., and Wang, H.-H., "Stability of Extremum Seeking Feedback for General Nonlinear Dynamic Systems," *Automatica*, Vol. 36, No. 4, 2000, pp. 595–601. doi:10.1016/S0005-1098(99)00183-1

[18] Dochain, D., Perrierb, M., and Guayc, M., "Extremum Seeking Control and Its Application to Process and Reaction Systems: A Survey," *Mathematics and Computers in Simulation*, Vol. 82, No. 3, 2011, pp. 369–380. doi:10.1016/j.matcom.2010.10.022

[19] Binetti, P., Ariyur, K., Krstic, M., and Bernelli, F., "Formation Flight Optimization Using Extremum Seeking Feedback," *Journal of Guidance, Control, and Dynamics*, Vol. 26, No. 1, 2003, pp. 132–142. doi:10.2514/2.5024

[20] Krieger, J., and Krstic, M., "Extremum Seeking Based on Atmospheric Turbulence for Aircraft Endurance," *Journal of Guidance, Control, and Dynamics*, Vol. 34, No. 6, 2011, pp. 1876–1885. doi:10.2514/1.53825

[21] Shin, Y., Calise, A., and Johnson, M., "Adaptive Control of Advanced Fighter Aircraft in Nonlinear Flight Regimes," *Journal of Guidance, Control, and Dynamics*, Vol. 31, No. 5, 2008, pp. 1464–1477. doi:10.2514/1.30213

[22] Finck, R. D., USAF Stability and Control Datcom, U.S. Air Force Wright Aeronautical Labs AFWAL-TR-83-3048, 1960.

[23] Gavilan, F., "Sistemas de control y guiado para vehículos aéreos no tripulados: diseño de algoritmos y sistemas embarcados," Ph.D. Thesis, Univ. de Sevilla, Seville, Spain, 2012.

[24] Gavilan, F., Acosta, J. A., and Vazquez, R., "Control of the Longitudinal Flight Dynamics of an UAV Using Adaptive Backstepping," *Proceedings of the 18th International Federation on Automatic Control World Congress*, IFAC Secretariat, Laxenburg, Austria, 2011, pp. 1892–1897.

[25] Gavilan, F., Vazquez, R., and Acosta, J. A., "Output-Feedback Control of the Longitudinal Flight Dynamics Using Adaptive Backstepping," *Proceedings of the 50th IEEE Conference on Decision and Control and European Control Conference*, IEEE Publ., Piscataway, NJ, 2011, pp. 6858–6863.

[26] Stevens, B. L., and Lewis, F. L., *Aircraft Control and Simulation*, 2nd ed., Wiley, Hoboken, NJ, 2003, pp. 114–115.

[27] Stenguel, R. F., *Fight Dynamics*, Princeton Univ. Press, Princeton, NJ, 2004, pp. 62–64.

[28] Krstic, M., and Kokotovic, P. V., "Lean Backstepping Design for a Jet Engine Compressor Model," *Proceedings of the IEEE Conference on Control Applications*, IEEE Publ., Piscataway, NJ, 1995, pp. 1047–1052.

[29] Teper, G. L., "Aircraft Stability and Control Data," NASA CR-96008, 1969.